

The Connection between Gamma-Ray Bursts and Extremely Metal-Poor Stars as Nucleosynthetic Probes of the Early Universe

K. Nomoto^{1,2}, N. Tominaga¹, M. Tanaka¹, K. Maeda², and H. Umeda¹

¹Department of Astronomy, University of Tokyo, Bunkyo-ku, Tokyo 113-0033, Japan
email: nomoto@astron.s.u-tokyo.ac.jp

²Institute for the Physics and Mathematics of the Universe, University of Tokyo, Kashiwa, Chiba 277-8582, Japan

Abstract.

The connection between the long GRBs and Type Ic Supernovae (SNe) has revealed the interesting diversity: (i) GRB-SNe, (ii) Non-GRB Hypernovae (HNe), (iii) X-Ray Flash (XRF)-SNe, and (iv) Non-SN GRBs (or dark HNe). We show that nucleosynthetic properties found in the above diversity are connected to the variation of the abundance patterns of extremely-metal-poor (EMP) stars, such as the excess of C, Co, Zn relative to Fe. We explain such a connection in a unified manner as nucleosynthesis of hyper-aspherical (jet-induced) explosions of Pop III core-collapse SNe. We show that (1) the explosions with large energy deposition rate, \dot{E}_{dep} , are observed as GRB-HNe and their yields can explain the abundances of normal EMP stars, and (2) the explosions with small \dot{E}_{dep} are observed as GRBs without bright SNe and can be responsible for the formation of the C-rich EMP (CEMP) and the hyper metal-poor (HMP) stars. We thus propose that GRB-HNe and the Non-SN GRBs (dark HNe) belong to a continuous series of BH-forming massive stellar deaths with the relativistic jets of different \dot{E}_{dep} .

Keywords. Galaxy: halo — gamma rays: bursts — nuclear reactions, nucleosynthesis, abundances — stars: abundances — stars: Population II — supernovae: general

1. Introduction

Among the most interesting recent developments in the study of supernovae (SNe) is the establishment of the Gamma-Ray Burst (GRB)-Supernova Connection (Woosley & Bloom 2006). Three GRB-associated SNe have been observed so far: GRB 980425/SN 1998bw (Galama *et al.* 1998, Iwamoto *et al.* 1998), GRB 030329/SN 2003dh (Stanek *et al.* 2003, Hjorth *et al.* 2003), and GRB 031203/SN 2003lw (Malesani *et al.* 2004). They are all very energetic supernovae, whose kinetic energy E exceeds 10^{52} erg, more than 10 times the kinetic energy of normal core-collapse SNe. In the present paper, we use the term 'Hypernova (HN)' to describe such a hyper-energetic supernova with $E_{51} = E/10^{51}$ erg $\gtrsim 10$ (Fig.1; Nomoto *et al.* 2004, Nomoto *et al.* 2006). The above three SNe associated with GRBs are called "GRB-HNe".

In contrast, "non-SN GRBs" (or *dark HNe*) have also been discovered (GRBs 060605 and 060614) (Fynbo *et al.* 2006, Gal-Yam *et al.* 2006, Della Valle *et al.* 2006, Gehrels *et al.* 2006). Upper limits to brightness of the possible SNe are about 100 times fainter than SN 1998bw. These correspond to upper limits to the ejected ^{56}Ni mass of $M(^{56}\text{Ni}) \sim 10^{-3}M_{\odot}$ (see, e.g., Nomoto *et al.* 2007 for prediction).

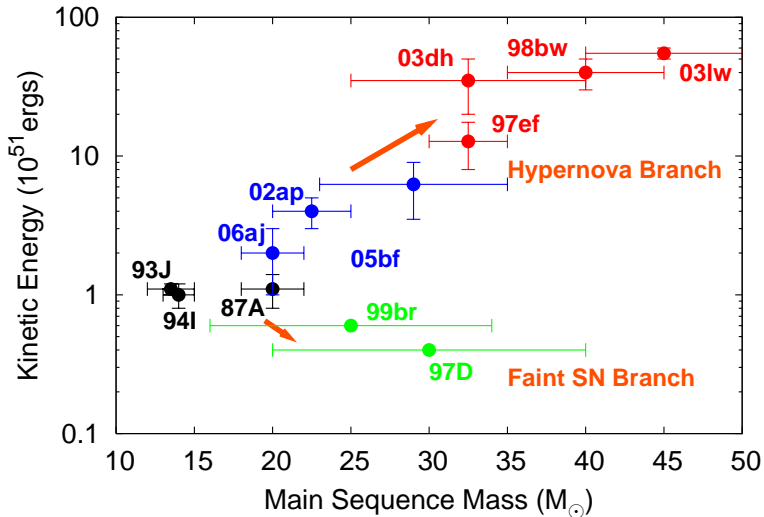


Figure 1. The kinetic explosion energy E as a function of the main sequence mass M of the progenitors for several supernovae/hypernovae. Hypernovae are the SNe with $E_{51} > 10$.

Such hypernovae and GRBs are also likely to be hyper-aspherical explosions induced by relativistic jet(s) as suggested from photometric and spectroscopic observations.

We calculate nucleosynthesis in such hyper-energetic and hyper-aspherical explosions and find that resultant abundance features show some important differences from normal supernova explosions (e.g., Maeda *et al.* 2002, Maeda & Nomoto 2003, Tominaga *et al.* 2007, Tominaga 2007). We show that such features can explain the peculiar abundance patterns observed in the extremely metal-poor (EMP), and hyper-metal-poor (HMP) halo stars (e.g., Hill, François, & Primas 2005, Beers & Christlieb 2005). This approach would lead to identifying the First Stars in the Universe, which is one of the important challenges of the current astronomy.

2. Nucleosynthesis in Jet-Induced Explosions

We calculate hydrodynamics and nucleosynthesis of the explosions induced by relativistic jets (*jet-induced explosions*) (Fig. 2) (Tominaga *et al.* 2007, Tominaga 2007). For the $40M_{\odot}$ stars (Umeda & Nomoto 2005, Tominaga, Umeda, & Nomoto 2007), the jets are injected at a radius $R_0 \sim 900$ km (corresponding to an enclosed mass of $M_0 \sim 1.4M_{\odot}$). The most important parameter in our models is the energy deposition rate \dot{E}_{dep} . We investigate the dependence of nucleosynthesis outcome on \dot{E}_{dep} for a range of $\dot{E}_{\text{dep},51} \equiv \dot{E}_{\text{dep}}/10^{51}\text{ergs s}^{-1} = 0.3 - 1500$. The diversity of \dot{E}_{dep} is consistent with the wide range of the observed isotropic equivalent γ -ray energies and timescales of GRBs (Amati *et al.* 2006 and references therein). Variations of activities of the central engines, possibly corresponding to different rotational velocities or magnetic fields, may well produce the variation of \dot{E}_{dep} .

The upper panel of Figure 3 shows the dependence of the ejected $M(^{56}\text{Ni})$ on \dot{E}_{dep} . Generally, higher \dot{E}_{dep} leads to the synthesis of larger $M(^{56}\text{Ni})$ in explosive nucleosynthesis because of higher post-shock densities and temperatures (e.g., Maeda & Nomoto 2003, Nagataki *et al.* 2006). If $\dot{E}_{\text{dep},51} \gtrsim 60$, we obtain $M(^{56}\text{Ni}) \gtrsim 0.1M_{\odot}$, which is consistent with the brightness of GRB-HNe. Some C+O core materials are ejected along the jet-direction, but a large amount of materials along the equatorial plane fall back (Fig. 2).

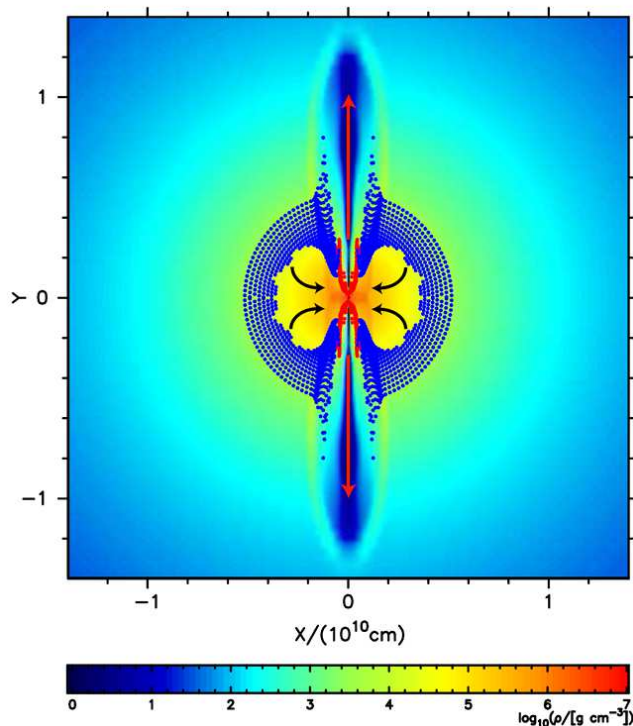


Figure 2. The density structure of the $40 M_{\odot}$ Pop III star explosion model of $\dot{E}_{\text{dep},51} = 15$ at 1 sec after the start of the jet injection. The jets penetrate the stellar mantle (*red arrows*) and material falls on the plane perpendicular to the jets (*black arrows*). The dots represent ejected Lagrangian elements dominated by Fe (^{56}Ni , *red*) and by O (*blue*).

For $\dot{E}_{\text{dep},51} \gtrsim 60$, the remnant mass is initially $M_{\text{rem}}^{\text{start}} \sim 1.5 M_{\odot}$ and grows as materials are accreted from the equatorial plane (Fig. 2). The final BH mass is generally larger for smaller \dot{E}_{dep} . The final BH masses range from $M_{\text{BH}} = 10.8 M_{\odot}$ for $\dot{E}_{\text{dep},51} = 60$ to $M_{\text{BH}} = 5.5 M_{\odot}$ for $\dot{E}_{\text{dep},51} = 1500$, which are consistent with the observed masses of stellar-mass BHs (Bailyn *et al.* 1998). The model with $\dot{E}_{\text{dep},51} = 300$ synthesizes $M(^{56}\text{Ni}) \sim 0.4 M_{\odot}$ and the final mass of BH left after the explosion is $M_{\text{BH}} = 6.4 M_{\odot}$.

For low energy deposition rates ($\dot{E}_{\text{dep},51} < 3$), in contrast, the ejected ^{56}Ni masses ($M(^{56}\text{Ni}) < 10^{-3} M_{\odot}$) are smaller than the upper limits for GRBs 060505 and 060614.

If the explosion is viewed from the jet direction, we would observe GRB without SN re-brightening. This may be the situation for GRBs 060505 and 060614. In particular, for $\dot{E}_{\text{dep},51} < 1.5$, ^{56}Ni cannot be synthesized explosively and the jet component of the Fe-peak elements dominates the total yields (Fig. 4). The models eject very little $M(^{56}\text{Ni})$ ($\sim 10^{-6} M_{\odot}$).

For intermediate energy deposition rates ($3 \lesssim \dot{E}_{\text{dep},51} < 60$), the explosions eject $10^{-3} M_{\odot} \lesssim M(^{56}\text{Ni}) < 0.1 M_{\odot}$ and the final BH masses are $10.8 M_{\odot} \lesssim M_{\text{BH}} < 15.1 M_{\odot}$. The resulting SN is faint ($M(^{56}\text{Ni}) < 0.01 M_{\odot}$) or sub-luminous ($0.01 M_{\odot} \lesssim M(^{56}\text{Ni}) < 0.1 M_{\odot}$).

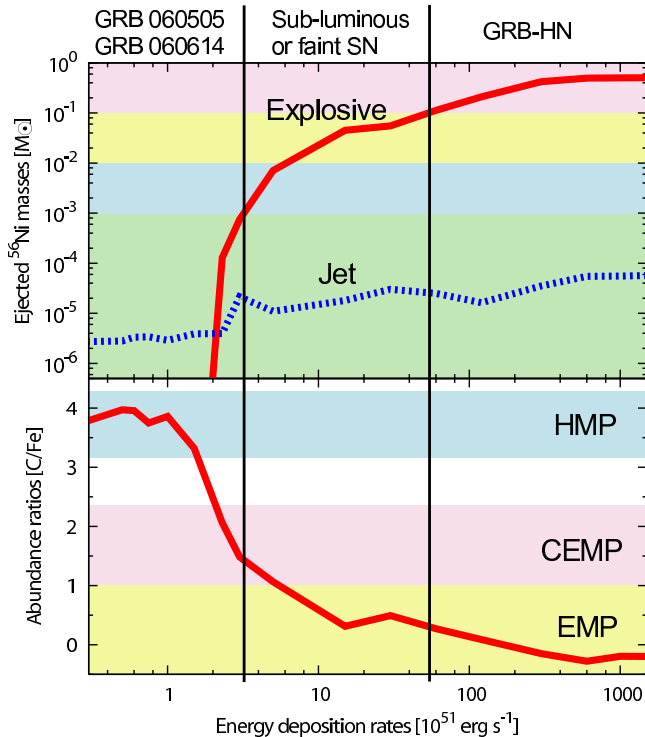


Figure 3. *Upper:* the ejected ^{56}Ni mass (*red*: explosive nucleosynthesis products, *blue*: the jet contribution) as a function of the energy deposition rate. The background color shows the corresponding SNe (*red*: GRB-HNe, *yellow*: sub-luminous SNe, *blue*: faint SNe, *green*: GRBs 060505 and 060614). Vertical lines divide the resulting SNe according to their brightness. *Lower:* the dependence of abundance ratio $[\text{C}/\text{Fe}]$ on the energy deposition rate. The background color shows the corresponding metal-poor stars (*yellow*: EMP, *red*: CEMP, *blue*: HMP stars).

3. Abundance Patterns of Extremely Metal-Poor Stars

Table 1 summarizes the abundance features of various EMP stars. In addition to HMP stars, we focus on the recently discovered first Ultra Metal-Poor (UMP) star (Norris *et al.* 2007) and the very peculiar Si-poor star (Cohen *et al.* 2007). Many of these EMP stars have high $[\text{Co}/\text{Fe}]$, suggesting the HN-connection.

3.1. C-rich Metal-Poor Stars (CEMP)

The lower panel of Figure 3 shows the dependence of the abundance ratio $[\text{C}/\text{Fe}]$ on \dot{E}_{dep} . Lower \dot{E}_{dep} yields larger M_{BH} and thus larger $[\text{C}/\text{Fe}]$, because the infall decreases the amount of inner core material (Fe) relative to that of outer material (C) (see also Maeda & Nomoto 2003). As in the case of $M(^{56}\text{Ni})$, $[\text{C}/\text{Fe}]$ changes dramatically at $\dot{E}_{\text{dep},51} \sim 3$.

The abundance patterns of the EMP stars are good indicators of SN nucleosynthesis because the Galaxy was effectively unmixed at $[\text{Fe}/\text{H}] < -3$ (e.g., Tumlinson 2006). They are classified into three groups according to $[\text{C}/\text{Fe}]$:

- (1) $[\text{C}/\text{Fe}] \sim 0$, normal EMP stars ($-4 < [\text{Fe}/\text{H}] < -3$, e.g., Cayrel *et al.* 2004);
- (2) $[\text{C}/\text{Fe}] \gtrsim +1$, Carbon-enhanced EMP (CEMP) stars ($-4 < [\text{Fe}/\text{H}] < -3$, e.g., CS 22949–37, Depagne *et al.* 2002);
- (3) $[\text{C}/\text{Fe}] \sim +4$, hyper metal-poor (HMP) stars ($[\text{Fe}/\text{H}] < -5$, e.g., HE 0107–5240, Christlieb *et al.* 2002, Bessell & Christlieb 2005; HE 1327–2326, Frebel *et al.* 2005).

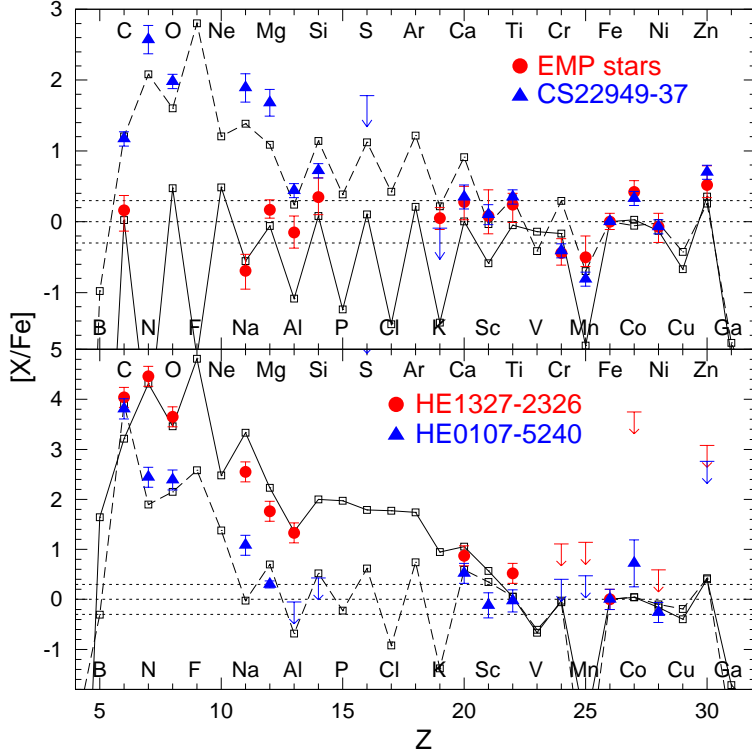


Figure 4. A comparison of the abundance patterns between the metal-poor stars and our models. *Upper:* typical EMP (red dots, Cayrel *et al.* 2004) and CEMP (blue triangles, CS 22949-37, Depagne *et al.* 2002) stars and models with $\dot{E}_{\text{dep},51} = 120$ (solid line) and $= 3.0$ (dashed line). *Lower:* HMP stars: HE 1327-2326, (red dots, e.g., Frebel *et al.* 2005), and HE 0107-5240, (blue triangles, Christlieb *et al.* 2002, Bessell & Christlieb 2005) and models with $\dot{E}_{\text{dep},51} = 1.5$ (solid line) and $= 0.5$ (dashed line).

Figure 4 shows that the abundance patterns of the averaged normal EMP stars, the CEMP star CS 22949-37, and the two HMP stars (HE 0107-5240 and HE 1327-2326) are well-reproduced by models with $\dot{E}_{\text{dep},51} = 120, 3.0, 1.5,$ and 0.5 , respectively. The model for the normal EMP stars ejects $M(^{56}\text{Ni}) \sim 0.2M_{\odot}$, i.e., a factor of 2 less than SN 1998bw. On the other hand, the models for the CEMP and the HMP stars eject $M(^{56}\text{Ni}) \sim 8 \times 10^{-4}M_{\odot}$ and $4 \times 10^{-6}M_{\odot}$, respectively, which are always smaller than the upper limits for GRBs 060505 and 060614. The N/C ratio in the models for CS 22949-37 and HE 1327-2326 is enhanced by partial mixing between the He and H layers during presupernova evolution (Iwamoto *et al.* 2005).

3.2. UMP Star HE 0557-4840 and CEMP-no Star HE 1300+0157

The abundance pattern of the first Ultra Metal-Poor (UMP) star (HE 0557-4840: Norris *et al.* 2007) is shown in Figure 5 and compared with the HN ($E_{51} = 20$) and SN ($E_{51} = 1$) models of the $25M_{\odot}$ stars. The Co/Fe ratio ($[\text{Co}/\text{Fe}] \sim 0$) requires a high energy explosion and the high $[\text{Sc}/\text{Ti}]$ and $[\text{Ti}/\text{Fe}]$ ratios require a high-entropy explosion. As shown in Figure 5 (upper), a HN model with a “low-density” modification (Tominaga *et al.* 2007) is in a good agreement with the abundance pattern of HE 0557-4840. The model indicates $M(^{56}\text{Ni}) \sim 10^{-3}M_{\odot}$ being similar to faint SN models for CEMP stars. The $[\text{Cr}/\text{Fe}]$ ratio in the model is much higher than that of HE 0557-4840.

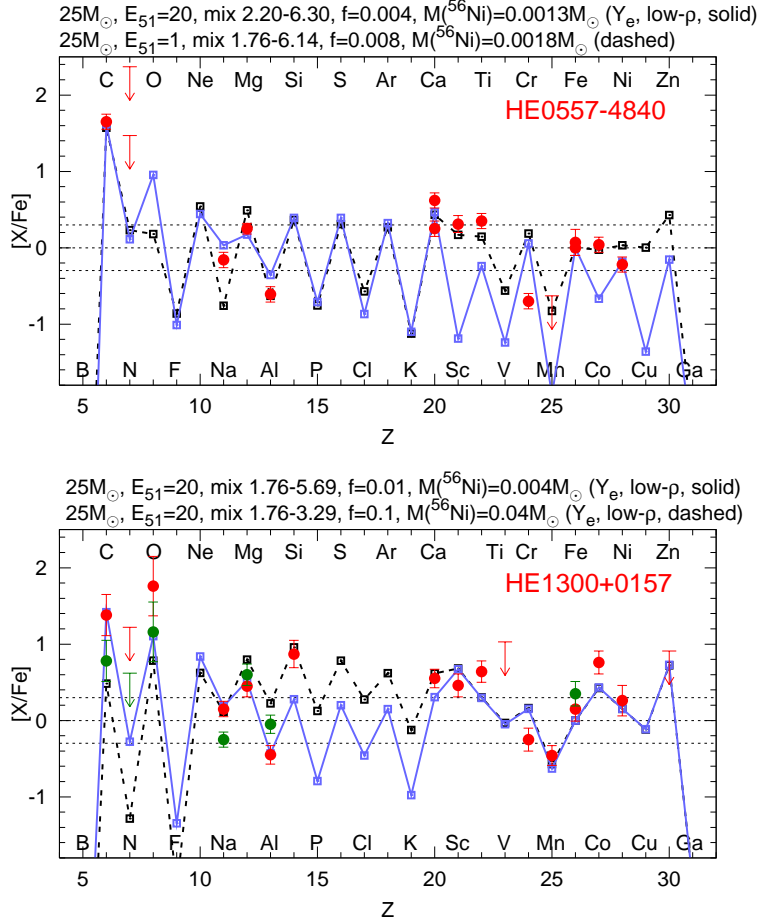


Figure 5. Comparisons of the abundance patterns between the mixing-fallback models and the UMP star HE0557–4840 (upper: Norris *et al.* 2007), and the CEP star HE1300+0157 (lower: Frebel *et al.* 2007).

Table 1. Metal-poor stars.

Name	[Fe/H]	Features	Reference
HE 0107–5240	–5.3	C-rich, Co-rich?, [Mg/Fe] ~ 0	Christlieb <i>et al.</i> 2002
HE 1327–2326	–5.5	C, O, Mg-rich	Frebel <i>et al.</i> 2005, Aoki <i>et al.</i> 2006
HE 0557–4840	–4.8	C, Ca, Sc, Ti-rich, [Co/Fe] ~ 0	Norris <i>et al.</i> 2007
HE 1300+0157	–3.9	C, Si, Ca, Sc, Ti, Co-rich	Frebel <i>et al.</i> 2007
HE 1424–0241	–4.0	Co, Mn-rich, Si, Ca, Cu-poor	Cohen <i>et al.</i> 2007
CS 22949–37	–4.0	C, N, O, Mg, Co, Zn-rich	Depagne <i>et al.</i> 2002
CS 29498–43	–3.5	C, N, O, Mg-rich, [Co/Fe] ~ 0	Aoki <i>et al.</i> 2004
BS 16934–002	–2.8	O, Mg-rich, C-poor	Aoki <i>et al.</i> 2007

The abundance pattern of the CEMP-no star (i.e., CEMP with no neutron capture elements) HE 1300+0157 (Frebel *et al.* 2007) is shown in Figure 5 (lower) and marginally reproduced by the hypernova model with $M_{\text{MS}} = 25M_{\odot}$ and $E_{51} = 20$. The large [Co/Fe] particularly requires the high explosion energy.

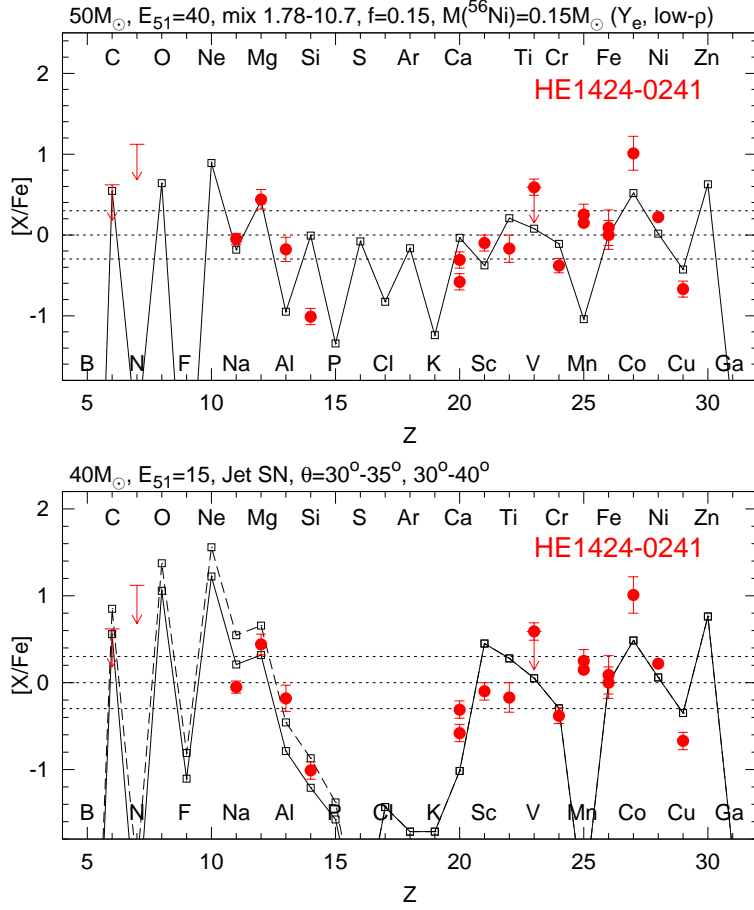


Figure 6. Comparisons between the abundance patterns of HE1424-0241 (Cohen *et al.* 2007) and the mixing-fallback model (upper), and the angle-delimited yields integrated over $30^{\circ} - 40^{\circ}$ (dashed line) and $30^{\circ} - 35^{\circ}$ (solid line) of the jet-induced SN model with $\dot{E}_{\text{dep}} = 1.2 \times 10^{53}$ ergs s^{-1} (lower).

3.3. Si-Poor Star: HE 1424-0241

The very peculiar Si-poor abundance pattern of HE 1424-0241 (Cohen *et al.* 2007) is shown in Figure 6 (upper) and compared with the model of $M_{\text{MS}} = 50M_{\odot}$ and $E_{51} = 40$. The high $[\text{Mg}/\text{Si}]$ ratio cannot be reproduced by this model. The peculiar abundance pattern of HE 1424-0241 is a challenge to the explosion models.

The angle-delimited yield provides a possibility to explain the high $[\text{Mg}/\text{Si}]$ and normal $[\text{Mg}/\text{Fe}]$. Figure 6 (lower) shows that the yields integrated over $30^{\circ} - 40^{\circ}$ or $30^{\circ} - 35^{\circ}$ reproduce the abundance pattern of HE 1424-0241. The yields consist of Mg in the inner region and Fe in the outer region.

Thus the most difficult pattern can be reproduced by the angular dependence of the yield. The high $[\text{Mg}/\text{Si}]$ and normal $[\text{Mg}/\text{Fe}]$ are realized if the heavy elements penetrate into the stellar mantle and expand laterally (i.e., the duration of the jet injection is long) and if Mg along the equatorial plane is not accreted onto the central region (i.e., \dot{E}_{dep} is large).

4. Concluding Remarks

We show that (1) the explosions with large energy deposition rate, \dot{E}_{dep} , are observed as GRB-HNe and their yields can explain the abundances of normal EMP stars, and (2) the explosions with small \dot{E}_{dep} are observed as GRBs without bright SNe and can be responsible for the formation of the CEMP and the HMP stars. We thus propose that GRB-HNe and GRBs without bright SNe belong to a continuous series of BH-forming massive stellar deaths with the relativistic jets of different \dot{E}_{dep} . The very peculiar Si-poor EMP star can also be explained by the angle-delimited yield.

References

- Amati, L., Della Valle, M., Frontera, F., *et al.* 2007, *A&A* 463, 913
Aoki, W., *et al.* 2004, *ApJ* 608, 971
Aoki, W., *et al.* 2006, *ApJ* 639, 897
Aoki, W., *et al.* 2007, *ApJ* 660, 747
Bailyn, C.D., Jain, R.K., Coppi, P., & Orosz, J.A. 1998, *ApJ* 499, 367
Beers, T., & Christlieb, N. 2005, *ARA&A* 43, 531
Bessell, M. S., & Christlieb, N. 2005, in V. Hill *et al.* (eds.), *From Lithium to Uranium*, Proc. IAU Symposium No. 228 (Cambridge: Cambridge Univ. Press), p. 237
Cayrel, R., *et al.* 2004, *A&A* 416, 1117
Christlieb, N., *et al.* 2002, *Nature* 419, 904
Cohen, J.G., *et al.* 2007, *ApJ* 659, L161
Della Valle, M., *et al.* 2006, *Nature* 444, 1050
Depagne, E., *et al.* 2002, *A&A* 390, 187
Fynbo, J.P.U., *et al.* 2006, *Nature* 444, 1047
Frebel, A., *et al.* 2005, *Nature* 434, 871
Frebel, A., *et al.* 2007, *ApJ* 658, 534
Galama, T., *et al.* 1998, *Nature* 395, 670
Gal-Yam, A., *et al.* 2006, *Nature* 444, 1053
Gehrels, N., *et al.* 2006, *Nature* 444, 1044
Hill, V., François, P., & Primas, F. (eds.) 2005, *From Lithium to Uranium: Elemental Tracers of Early Cosmic Evolution*, Proc. IAU Symp. No. 228 (Cambridge: Cambridge Univ. Press)
Hjorth, J., *et al.* 2003, *Nature* 423, 847
Iwamoto, K., Mazzali, P.A., Nomoto, K., *et al.* 1998, *Nature* 395, 672
Iwamoto, N., Umeda, H., Tominaga, N., Nomoto, K., & Maeda, K. 2005, *Science* 309, 451
Maeda, K., Nakamura, T., Nomoto, K., *et al.* 2002, *ApJ* 565, 405
Maeda, K., & Nomoto, K. 2003, *ApJ* 598, 1163
Malesani, J., *et al.* 2006, *ApJ* 609, L5
Nagataki, S., Mizuta, A., & Sato, K. 2006, *ApJ* 647, 1255
Nomoto, K., *et al.* 2004, in C.L. Fryer (ed.), *Stellar Collapse* (Astrophysics and Space Science: Kluwer), p. 277 (astro-ph/0308136)
Nomoto, K., *et al.* 2006, *Nuclear Phys A* 777, 424 (astro-ph/0605725)
Nomoto, K., *et al.* 2007, *Nuovo Cimento* 121, 1207 (astro-ph/0702472)
Norris, J. E., *et al.* 2007, *ApJ* 670, 774
Stanek, K.Z., *et al.* 2003, *ApJ* 591, L17
Tominaga, N., Tanaka, M., Nomoto, K., *et al.* 2005, *ApJ* 633, L97
Tominaga, N., Maeda, K., Umeda, H., Nomoto, K., Tanaka, *et al.* 2007, *ApJ* 657, L77
Tominaga, N., Umeda, H., & Nomoto, K. 2007, *ApJ* 660, 516
Tominaga, N. 2007, *ApJ* submitted (arXiv:0711.4815)
Tumlinson, J. 2006, *ApJ* 641, 1
Umeda, H., & Nomoto, K. 2002, *ApJ* 565, 385
Umeda, H., & Nomoto, K. 2005, *ApJ* 619, 427
Woosley, S. E., & Bloom, J.S. 2006, *ARA&A* 44, 507